

OPEN ACCESS

The Effect of Electric Fields on the Structure of Water/Acetonitrile Mixtures

To cite this article: Anastasios I. Sourpis *et al* 2023 *J. Electrochem. Soc.* **170** 083508

View the [article online](#) for updates and enhancements.

You may also like

- [Breath testing and personal exposure—SIFT-MS detection of breath acetonitrile for exposure monitoring](#)
Malina Storer, Kirsty Curry, Marie Squire et al.

- [Millimeter-wave gas spectroscopy for breath analysis of COPD patients in comparison to GC-MS](#)
Nick Rothbart, Victoria Stanley, Rembert Koczulla et al.

- [Acetonitrile Contamination and Recovery of Pemfcs](#)
Yunfeng Zhai and Jean St-Pierre

Investigate your battery materials under defined force!
The new PAT-Cell-Force, especially suitable for solid-state electrolytes!



- Battery test cell for force adjustment and measurement, 0 to 1500 Newton (0-5.9 MPa at 18mm electrode diameter)
- Additional monitoring of gas pressure and temperature

www.el-cell.com +49 (0) 40 79012 737 sales@el-cell.com

EL-CELL[®]
electrochemical test equipment





The Effect of Electric Fields on the Structure of Water/Acetonitrile Mixtures

Anastasios I. Sourpis,^{1,z} Nancy C. Forero-Martinez,^{1,2} and Friederike Schmid^{1,z}

¹Institut für Physik, Johannes Gutenberg-Universität Mainz, 55099 Mainz, Germany

²Max Planck Institute for Polymer Research, 55128 Mainz, Germany

We study the effect of macroscopic electric fields on the structure of water/acetonitrile mixtures at high acetonitrile content by molecular dynamics simulations. We find that the linear response regime extends up to roughly 0.1 V nm^{-1} in these mixtures, then nonlinear behavior sets in. The most pronounced nonlinear effect of an electric field is a change of relative orientations of neighboring acetonitrile molecules, from predominantly antiparallel to predominantly parallel. Nevertheless, the hydrogen bond network topology remains remarkably stable and conserves its overall properties in the whole range of considered applied fields up to 0.5 V nm^{-1} , which is far beyond the dielectric breakdown limit of pure water. Additionally, we report on a comparison of simulation results at zero field with experimental results and available ab-initio data using four different recently proposed acetonitrile force fields, where we find that the force field by Kowsari and Tohidifar [J. Comput. Chemistry 39, 1843, 2018] performs best. Furthermore, we demonstrate that analyzing the hydrogen bond network can be a useful tool in investigating the formation and structure of water nanodomains and their confinement by an acetonitrile matrix in water/acetonitrile mixtures. © 2023 The Author(s). Published on behalf of The Electrochemical Society by IOP Publishing Limited. This is an open access article distributed under the terms of the Creative Commons Attribution 4.0 License (CC BY, <http://creativecommons.org/licenses/by/4.0/>), which permits unrestricted reuse of the work in any medium, provided the original work is properly cited. [DOI: 10.1149/1945-7111/acef61]



Manuscript submitted May 15, 2023; revised manuscript received July 27, 2023. Published August 23, 2023. *This paper is part of the JES Focus Issue on Multiscale Modeling, Simulation and Design: In Honor of Ralph E. White.*

Supplementary material for this article is available [online](#)

Liquid mixtures of water and acetonitrile are commonly used as solvent media in a variety of applications such as chromatography, organic synthesis, and electrochemistry. Liquid acetonitrile (CCN) is an aprotic amphiphilic molecule with a large dipole moment, which is a good solvent for many solutes, both polar and non-polar, and also mixes reasonably well with protic solvents such as water. For these reasons, CCN liquids and aqueous CCN solutions have been studied intensely for many decades¹ by experiments (e.g. NMR, spectroscopy, X-ray scattering),^{2–10} theory,^{11–13} and simulations,^{5,8,10,14–27} and a number of force fields have been proposed that are specifically optimized for CCN.^{28–35}

Among others, these studies have revealed a tendency of CCN to form clusters or small domains in water (so-called microheterogeneities)^{9,17,21} in the concentration regime of 20%–75% CCN,^{1,9} and pronounced orientational correlations between neighboring CCN molecules.^{10–12,21,23} The exact nature of correlation found in simulations somewhat depends on the force field: Earlier studies reported the formation of head-to-head dimers,^{11,12} whereas more recent studies suggested a preference for antiparallel orientations and head-tail orientations where two neighbor CCN are perpendicular to each other.^{10,21,23} Also, the hydrogen bond distribution in water/CCN mixtures has been studied by various authors.^{4,5,15,36} Since CCN is aprotic, such studies give insight into the connectivity of water in water/CCN mixtures, which should have an impact on the proton transport in these fluids.

Studies of proton transfer phenomena in water mixtures are particularly interesting in hydrogen bonded systems. In particular, the effect of an external electric field on ethanol/water and methanol/water mixtures and their neat components has been studied via detailed ab-initio molecular dynamics simulations.^{37–41} These results show changes in the ionic conductivity of mixed systems in comparison to neat systems, negligible changes in the H-bond structure,³⁹ changes in probability distributions of α -helix H-bond characteristic lengths⁴² and an activation of chemical processes^{39,43–45} with increasing electric field.

In the case of water/CCN mixtures, with few exceptions,^{24,27} the vast majority of studies have considered equilibrium liquids. In view of the wide use of CCN mixtures in electrochemistry, studies of the

impact of electric fields on their structural properties are highly desirable. As a contribution to filling this gap, the present work presents a molecular dynamics study of the effect of externally imposed macroscopic electric fields on water/CCN mixtures. Since the choice of force field can have a critical influence on simulation results, we have first spent some effort into assessing and comparing different force fields. To this end, we have carried out simulations at zero electric field using different force fields for a range of concentrations and compared the predicted thermodynamic and structural quantities to known experimental values and ab-initio results.²¹ Based on this study, we have then selected one force field (Kowsari and Tohidifar³³) and focused on experimentally relevant mixtures with a high CCN content (75%) and studied them over a wide range of electric field strengths, ranging from the linear response regime to the strongly nonlinear regime. Our main findings can be summarized as follows: High electric fields significantly affect the relative orientation of neighboring CCN molecules. Interestingly, however, the structure of the hydrogen bond network is remarkably robust and hardly changes even in the nonlinear regime.

Our paper is organized as follows. In the next section, we describe the simulation methods and the main analysis tools; Additional information can be found in the supplementary information (SI). Then, in Comparison of Force Fields section, we discuss the results of the force field comparison, which motivates the choice of force field³³ used for the main study. The results of the main study are presented in Impact of Electric Fields on CCN-Water Mixtures section. We conclude with a summary in Summary and Conclusions section.

Methods

We performed classical atomistic molecular dynamics (MD) simulations of pure CCN and CCN-water mixtures in the bulk (periodic boundary conditions) with different CCN concentrations (x_{CCN}) using the GROMACS 2018.1 simulation package.⁴⁶ Unless stated otherwise, we use the rigid SPC force field⁴⁷ for water, the force field by Kowsari and Tohidifar³³ for CCN, and the Lorentz-Berthelot mixing rules to determine the mixed potential terms. The Comparison of Force Fields section also shows results at $E = 0$ for other CCN force fields^{30–33} and for the TIP4P water model⁴⁸ for comparison.

^zE-mail: asourpis@uni-mainz.de; friederike.schmid@uni-mainz.de

The macroscopic electric field \mathbf{E} points in the x direction. It contributes an extra force $q_i\mathbf{E}$ in the equations of motion of atoms i with charges q_i . We note that \mathbf{E} is different from the so-called “applied field” \mathbf{E}_0 , which is also sometimes used in the literature to characterize electric field effects. In a setting where the electric field \mathbf{E} is assumed to be generated by a parallel plate capacitor, \mathbf{E}_0 denotes the electric field in a reference capacitor with same geometry and same surface charges, but which is empty inside instead of being filled with the (dielectric) CCN-water mixture. (In an empty reference capacitor with same geometry and same applied *voltage*, the electric field is still \mathbf{E}). In order to perform molecular dynamics simulations at constant \mathbf{E}_0 , one must add a force term that couples to the polarization of the system.^{49–51} In our system, however, we found such simulations to suffer from large finite size effects, therefore we only show results for constant \mathbf{E} here.

The numbers of CCN and water molecules depend on the CCN concentration and were chosen such that, at the pressure of 1 bar, simulation boxes roughly had the size $5 \times 5 \times 5 \text{ nm}^3$ (see equilibration protocol below). For example, simulations at $x_{CCN} = 0.75$ correspond to 1216 CCN molecules and 406 water molecules, while 675 CCN molecules and 2028 water molecules were used in simulations at $x_{CCN} = 0.25$.

The time step used in the simulations was 1 fs. The LINear Constraint Solver (LINCS) algorithm⁵² was used to constrain bonds involving hydrogen in the CCN molecule. This was done to improve the stability, since simulations with the Koverga potential³² were found to sometimes crash if such constraints were not applied. The temperature was kept constant using the V-rescaling coupling method⁵³ with a relaxation time constant of 0.2 ps. Simulations at constant pressure (NPT) were done using the Parrinello-Rahman barostat with a time constant of 2.0 ps. Short range interactions such as the van-der-Waals interactions were cut off at 1.4 nm. The long-range electrostatic interactions were evaluated using the particle mesh Ewald (PME) method⁵⁴ with parameters 1.4 nm for the short-range part and grid spacing 0.12 nm for the Fourier part, using a fourth order interpolation scheme. The long-range forces and the Verlet lists used for neighbor searching were updated every 10 fs.

All simulations were initialized by first filling a simulation box with the desired number of CCN molecules from a single CCN configuration taken from the Protein Data Bank⁵⁵ using the PACKMOL software.⁵⁶ Geometric overlapping was eliminated via an energy minimization step using the steepest descent algorithm. The CCN system was then solvated with water molecules using GROMACS, followed by another energy minimization step. The energy minimization steps were done at zero electric field. Then the electric field was turned on, if applicable, and the systems were equilibrated via a series of alternating simulations at constant volume (NVT ensemble) and constant pressure (NPT ensemble): (i) An initial equilibration over 10 ns in the NVT ensemble at $T = 298 \text{ K}$; (ii) An NPT simulation over 25–35 ns at the pressure of 1.0 atm, in order to adjust the size of the simulation box; (iii) A final equilibration in the NVT ensemble over 25 ns. Production runs had a total length of 100 ns. In the force field comparison simulations described in Comparison of Force Fields section, the initial equilibration (i) included an NVT simulation of 10 ns at temperature $T = 400 \text{ K}$ followed by an annealing procedure from $T = 400 \text{ K}$ to $T = 298 \text{ K}$ over 10 ns.

After equilibration, NVT simulations over 100 ns were carried out for data collection and analysis (5–10 ns in the force field comparison). To assess the characteristic time scales of our system, we have computed the dipole time autocorrelation function for CCN molecules, see Fig. 1. It is found to decay to zero within 100 ps. The total simulation time in the production runs thus corresponds to more than 10^4 rotational relaxation times of CCN. In these, we used the last 15 ns for determining radial distribution functions, the last 25 ns for determining combined distribution functions (see below), and the full 100 ns for carrying out the analysis of hydrogen bond networks.

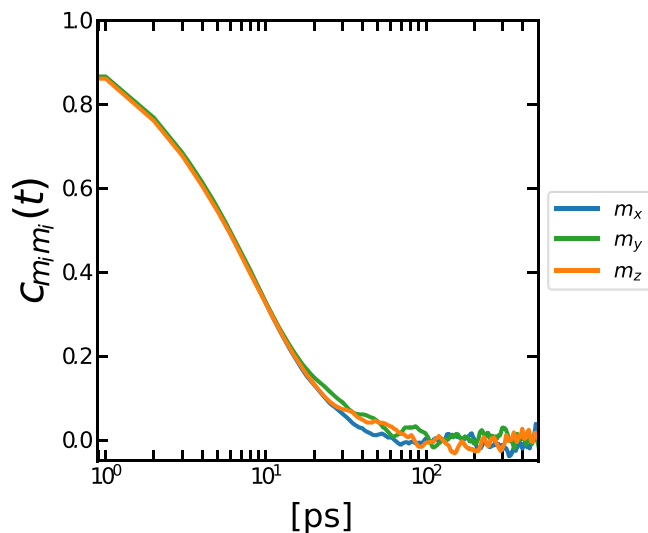


Figure 1. Autocorrelation function of CCN dipoles at zero electric field and CCN concentration $x_{CCN} = 0.75$. This simulation was done using the Kowsari force field³³ and SPC water.

Specifically, the radial distribution function of particles A and B is defined by

$$g_{AB}(r) = \frac{\rho_B(r)}{\langle \rho_B \rangle} = \frac{1}{\langle \rho_B \rangle} \frac{1}{N_A} \sum_{i \in A} \sum_{j \in B} \frac{\delta(r_{ij} - r)}{4\pi r^2}, \quad [1]$$

where $\rho_B(r)$ is the particle density of type B at a distance r around particle A . The normalization factor $\langle \rho_B \rangle$ is determined from the particle density of type B particles, averaged over all spheres around particles A with radius $r_{\max} = L/2$ where L is the simulation box length.

As another quantity to characterize the local structure of our fluids, we calculate the combined distribution function (CDF) of angular and radial correlations of CCN molecules. We analyze the last 25 ns of the production runs to obtain the CDF using the Travis trajectory analyzer.⁵⁷ The CDF is defined as:

$$g_{CDF}(r, \theta) = \frac{1}{N} \sum_i \sum_j \langle \delta(r - r_{ij}) \delta(\theta - \theta_{ij}) \rangle, \quad [2]$$

where r_{ij} is the distance between the center of masses of the i th and j th CCN molecules and the mutual orientation is defined by θ_{ij} , the angle between CCN “molecular” vectors. These vectors are defined for each CCN molecule as the vector connecting the carbon atom of the CH_3 group with the nitrogen atom.

Comparison of Force Fields

As mentioned in the introduction, several CCN force fields have been proposed in the literature,^{28–33} both united-atom models²⁹ and all-atom models with explicit hydrogen.^{28,30–33} In preparation of our study, we have thus compared the four more recently proposed force fields^{30–33} by carrying out simulations of systems with different CCN concentrations at zero electric field and comparing the structural and thermodynamic properties to experimental data and available ab-initio simulations.²¹ In addition, we have also compared results obtained with two different established water models, namely the three-site rigid SPC model⁴⁷ and the four-site TIP4P model.⁴⁸

All CCN models considered in this work are all-atom models and use the AMBER functional form.⁵⁸ The intramolecular interactions

include harmonic bonding and bending contributions, but no torsional potential and the non-bonded potentials include Lennard-Jones and Coulomb potentials. The force fields by Grabuleda et al.³⁰ and Nikitin and Lyubartsev³¹ are based on the AMBER model parameters and were tuned to either fit structural properties and density of pure CCN or reproduce experimental CCN-water mixture densities, the heat of evaporation and dielectric properties. Kovrega et al.³² developed an entirely new set of parameters to focus on the structural, dynamic, and thermodynamic properties of pure CCN. Most recently, Kowsari et al.³³ recalibrated the AMBER-based models to reach an agreement with dynamical properties such as the self-diffusion coefficient and thermodynamic properties of pure CCN while providing an appropriate qualitative description of the liquid CCN structure.

Density.—We begin with comparing the density of the mixtures at different CCN mole fractions x_{CCN} as obtained with the different force fields. The results are given in Table I. The best agreement with experiments is obtained with the Nikitin and the Kowsari force fields. Specifically, the results for the Kowsari force field combined with TIP4P water are in excellent agreement with the experimentally reported density values for all liquid-water mixtures except pure CCN. When combined with the SPC water model, the agreement between simulations and experiment is still very good.

Radial distribution functions.—Next, we consider the radial distribution functions (RDFs) (see Eq. 1), which allow us to understand how CCN and water molecules are, on average, radially packed with respect to each other.

Figures 2, 3 and 4 show selected RDFs for atom pairs between CCN and water molecules, comparing ab-initio simulations of Chen and Sit²¹ and our results obtained with the classical force fields^{30–33} and SPC water. (Additional data for RDFs can be found in the SI). These data can be used to evaluate our classical force fields.

In the case of the correlation function involving nitrogen (Figs. 2 and 3), all force fields roughly capture the basic structure of the RDFs and the positions of the peaks and minima. The height of the first peak is generally too high in the simulations with the Nikitin and Kovrega force fields^{31,32} and lowest in the simulations with the Kowsari force field.³³ At high CCN concentrations, the RDFs obtained with the Kowsari force field are in very good agreement with the ab-initio reference data. In the case of the correlation functions H-O_W between CCN hydrogen and water oxygen, the comparison of classical force field simulations with the ab-initio reference simulation is less favorable: The RDFs obtained from classical simulations are much more structured than the reference ones from the ab-initio simulations. In particular, they exhibit a peak at distance $r = 0.25$ nm for all CCN concentrations which is absent in the ab-initio simulations. However, this peak is less pronounced in the simulations with the Kowsari force field³³ than in the other simulations.

We conclude that the Kowsari force field³³ captures the local structure of water/CCN mixtures better than the other force fields and therefore choose to use this force field for the subsequent

studies that will be described in the next section. For reasons of computational efficiency, we combine this with the SPC water model, which is computationally much less expensive than the TIP4P water model and produces less noisy data in runs of similar length.

Impact of Electric Fields on CCN-Water Mixtures

We turn to discuss the effect of macroscopic electric fields on the properties of CCN/water mixtures. Here, we focus on systems with the CCN mole fraction $x_{CCN} = 0.75$, i.e. high CCN content, a composition that is interesting for use in electrolysis cells. As discussed in the previous section, we use the Kowsari CCN force field³³ in combination with the SPC water model. For the convenience of the reader, the force field parameters of the CCN force field are summarized in Tables S1 in SI.

Polarization.—As our system contains no free charges, but molecules with a large dipole moment \mathbf{m}_i , the most obvious effect of a macroscopic field \mathbf{E} is to orient the dipoles. We define the total dipole moment as $\mathbf{M} = \sum_i \mathbf{m}_i$ and also consider separately the contributions \mathbf{M}_{CCN} and \mathbf{M}_{H_2O} of acetonitrile and water. The polarization of the system (in the absence of free charges) is then given by $\mathbf{P} = \mathbf{M}/\Omega$, where Ω is the volume of the system.

Since the system contains no free charges, just well-defined dipoles, the additional electrostatic energy associated with a spatially homogeneous electric field \mathbf{E} can simply be written as⁵⁹ $\Delta H_{\mathbf{E}} = -\sum_i \mathbf{E} \cdot \mathbf{m}_i = -\mathbf{E} \cdot \mathbf{M}$, and the total energy of a given configuration \mathcal{C} is given by

$$H(\mathcal{C}) = H_0(\mathcal{C}) - \mathbf{E} \cdot \mathbf{M}. \quad [3]$$

Here $H_0(\mathcal{C})$ refers to the energy of the same configuration \mathcal{C} in the absence of a macroscopic field. This expression (3) also remains valid if the amplitudes $|\mathbf{m}_i|$ of molecular dipoles are affected by the electric field and even if the molecular dipoles are induced by the field. We note that the situation is more complicated if a system contains free charges such as ions. In this case the correct expression for the polarization \mathbf{P} is less obvious and the treatment of periodic boundary conditions requires extra care.^{60,61}

For small macroscopic electric fields, the energy contribution (3) can be treated as a perturbation and linear response theory can be applied. In the linear regime, one thus expects the thermal average of the polarization to be given by

$$\langle \mathbf{P} \rangle_{linear} = \frac{\beta \mathbf{E}}{\Omega} \langle \mathbf{M} \mathbf{M} \rangle_{\mathbf{E}=0} \quad [4]$$

where $\beta = 1/k_B T$ is the Boltzmann factor and $\mathbf{M} \mathbf{M}$ refers to the tensor product $M_i M_j$. The corresponding equation also holds for the individual contributions of water and CCN to the total polarization if \mathbf{M} is replaced by \mathbf{M}_{H_2O} and \mathbf{M}_{CCN} , respectively.

Figure 5 shows the simulation results for the polarization (symbols) and compares them with the linear response prediction, Eq. 4. From these curves, one can infer that the linear regime extends

Table I. Density (kg/m³) at pressure 1 bar obtained from simulations with different CCN and water force fields as indicated and compared to experiments.

Force field x_{CCN}	0.10	0.50	0.90	neat CCN
Kowsari ³³ /SPC ⁴⁷	939.7 ± 0.03	840.6 ± 0.1	795.6 ± 0.1	788.6 ± 0.3
Kowsari ³³ /TIP4P ⁴⁸	957.8 ± 0.1	845.6 ± 0.1	793.8 ± 0.1	788.6 ± 0.1
Kovrega ³² /SPC ⁴⁷	938.3 ± 0.06	834.3 ± 0.1	779.6 ± 0.2	770.7 ± 0.2
Kovrega ³² /TIP4P ⁴⁸	956.8 ± 0.03	842.0 ± 0.2	781.0 ± 0.1	770.7 ± 0.2
Nikitin ³¹ /SPC ⁴⁷	933.3 ± 0.04	846.0 ± 0.1	789.3 ± 0.1	773 ± 5 ³¹
Grabuleda ³⁰ /SPC ⁴⁷	922.2 ± 0.09	796.0 ± 0.07	742.2 ± 0.06	735.3 ± 5 ³⁰
Experiment ²	958.6	845.1	786.3	776.7

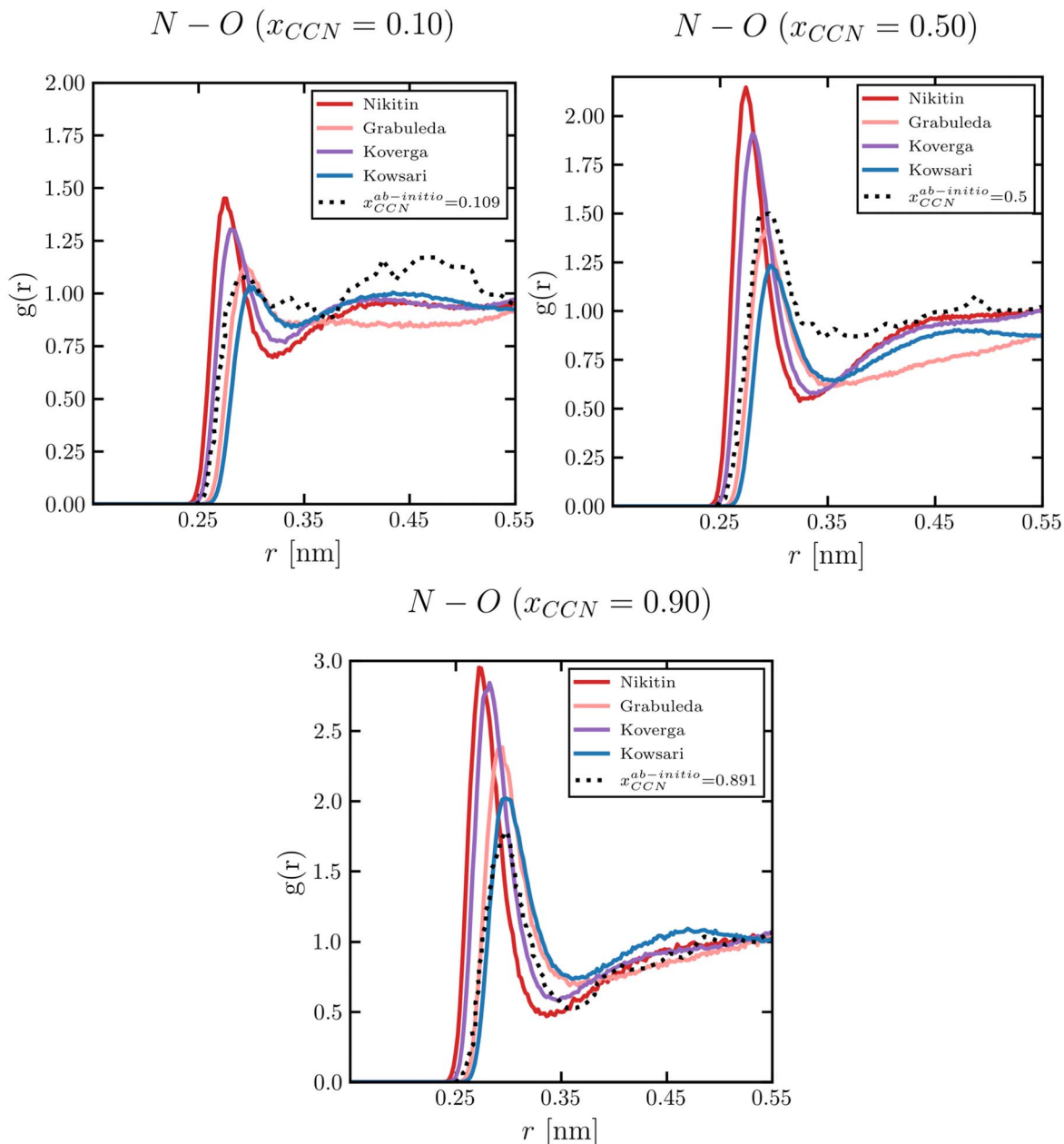


Figure 2. Radial distribution function of nitrogen N of acetonitrile and the oxygen O of water for different mole fraction as indicated for each plot, where force fields Nikitin³¹ Grabuleda,³⁰ Kalugin³² Kowsari³³ are compared to ab-initio results.²¹

up to roughly $|\mathbf{E}| \sim 0.1 \text{ V nm}^{-1}$. In the nonlinear regime, the curves for the polarization versus macroscopic field flatten. The crossover from linear to nonlinear becomes even clearer if one inspects the susceptibility $\chi(E)$, defined via $\mathbf{P} = \varepsilon_0 \chi(E) \mathbf{E}$ as the ratio of the polarization and the macroscopic field, which is shown in Fig. 6a as a function of E . It is initially constant ($\chi \approx 35$) and then decays with a quasi constant slope ($\chi(E) \approx 38 - 24 E \text{ nm/V}$) for field amplitudes higher than $E \sim 0.15 \text{ V/nm}$. Comparing the corresponding dielectric constant in the linear regime $\varepsilon_r = 1 + \chi \approx 36$, with the experimental value⁶² for acetonitrile/water mixtures at 75% CCN and temperature 25° , $\varepsilon_{r,\text{exp}} \approx 45$, one finds that it is of similar order, albeit a bit too low. The difference can partly be attributed to the fact that the simulations can only capture the reorientation contribution to ε , since we use a non-polarizable force field. In the nonlinear regime, the dielectric constant, defined via $\mathbf{D} = \varepsilon_r \varepsilon_0 \mathbf{E}$, is still isotropic and decreases with E following $\varepsilon_r(E) = 1 + \chi(E)$ (see also Eq. (22) in Ref. 50). However, the electrostatic interactions between free

charges in the system are governed by an effective dielectric tensor which is anisotropic (see SI for the derivation). Its components are given by $\varepsilon_{r,\text{eff}}^\perp = \varepsilon_r$ perpendicular to the macroscopic field, and $\varepsilon_{r,\text{eff}}^\parallel = 1 + \chi^d(E)$ parallel to the field, where χ^d is the differential susceptibility, $\chi^d(E) = \frac{1}{\varepsilon_0} dP/dE$. Figure 6b shows ε_r along with $\varepsilon_{r,\text{eff}}^\parallel$ and $\varepsilon_{r,\text{eff}}^\perp$. We note that $\varepsilon_{r,\text{eff}}^\parallel$ almost decays to one at high macroscopic fields E_x . This is consistent with the results of Daniels et al. for pure CCN,²⁴ who exploited the fluctuation relation $\chi^d \propto \langle \mathbf{P}^2 \rangle_E - \langle \mathbf{P} \rangle_E^2$ and calculated $\varepsilon_{r,\text{eff}}^\parallel$ directly from the polarization fluctuations.

We should note that the highest fields in Fig. 5a most likely exceed the dielectric strength of the mixture, i.e. the field amplitude where dielectric breakdown sets in. The dielectric strength of pure water is around $|\mathbf{E}|_{db} \sim 0.07 \text{ V nm}^{-1}$ in the bulk and can reach values of $|\mathbf{E}|_{db} \sim 0.4 \text{ V/nm}$ or more in narrow gaps.⁶³

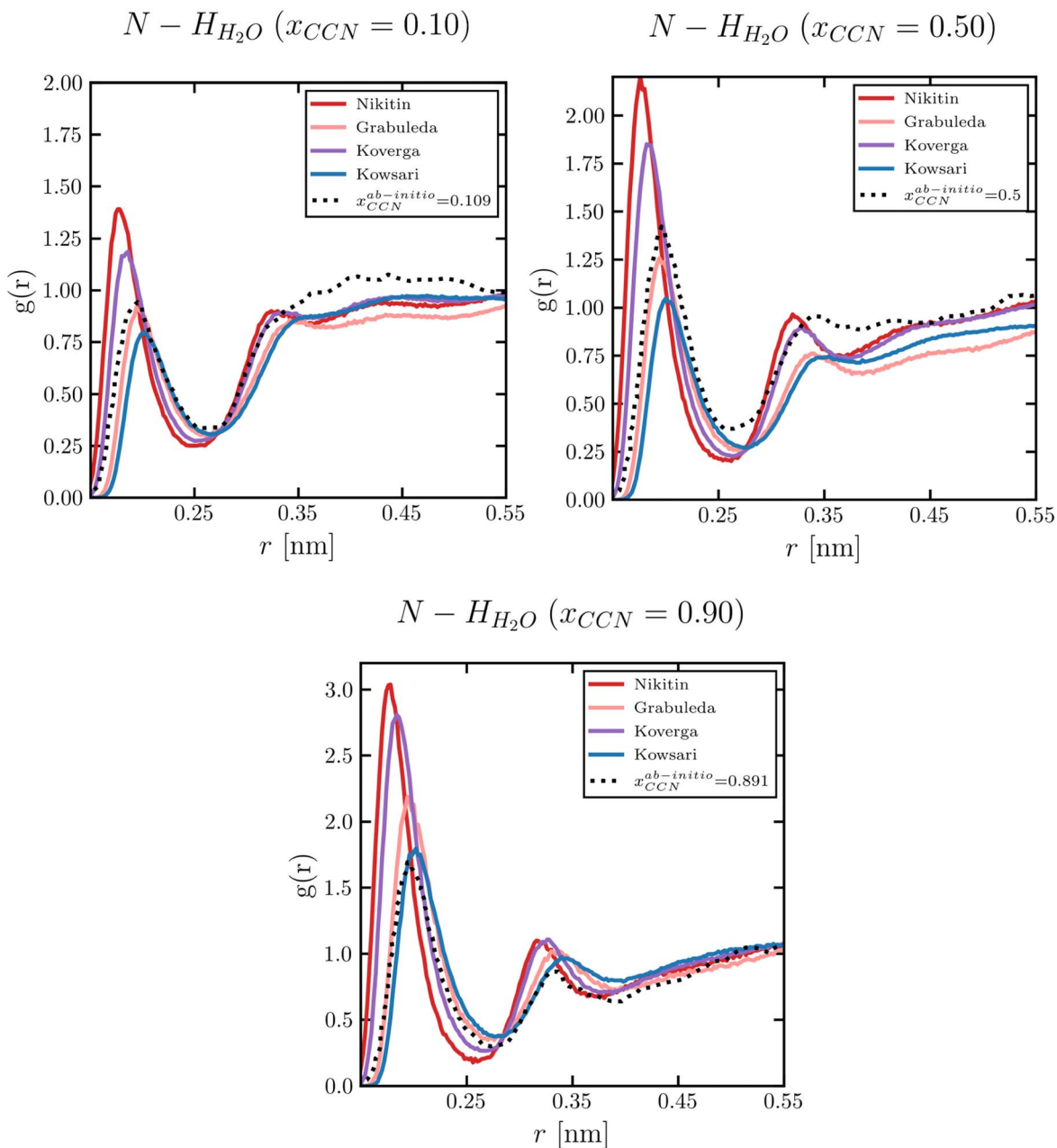


Figure 3. Same as Fig. 2 for nitrogen atoms in CCN and hydrogen atoms in water.

Local structure and correlations.—Having identified the linear response regime, we now search for signatures of nonlinear behavior in the local correlations of the water/CCN mixture. Figure 7 shows radial distribution functions $g(r)$ for selected atom pairs, namely, nitrogen/hydrogen water and nitrogen/nitrogen, over a wide range of applied electric fields \mathbf{E} . The influence of the electric field on $g(r)$ turns out to be almost negligible as also observed in methanol/water mixtures.³⁹ The different curves are almost identical in the case of atom pairs between CCN and water, and still very close to each other in the case of atom pairs between two CCN molecules. The pair distribution functions of other atom pairs, shown in SI, confirm this picture.

This however changes when we inspect the orientational correlations of CCN molecules. As discussed in the introduction, experimental as well as computational studies suggest that neighboring CCN molecules have a tendency to adopt an antiparallel orientation, regardless of whether they are in a pure or solvated state.^{10,21–23,26,32}

We use the combined distribution function (CDF) of angular and radial correlations to gain insight into the mutual orientation of the CCN molecules and how the distance between their center of masses affects these orientations, see Eq. 2 in Methods section. The CDF allow us to understand how the molecules arrange not only in a radial manner, but also how they orient relative to each other. We evaluate this function up to a distance of 0.6 nm, corresponding to the onset of the first minimum in the radial distribution function of the center of masses of CCN (Fig. S12 in SI). Figure 8 shows our results for zero applied field, $\mathbf{E} = 0$. The CDF, $g_{CDF}(r, \theta)$, has a maximum at $\theta = 180^\circ$ and $r \sim 0.37$ nm, corresponding to configurations where the closest neighbors are at a distance of around 0.37 nm and the mutual orientation of CCN molecules is antiparallel. Earlier studies of pure CCN liquids^{10,23} have reported a second peak suggesting an additional preference for perpendicular orientations with head-tail orientation. This peak is absent in our simulations of CCN/water mixtures.

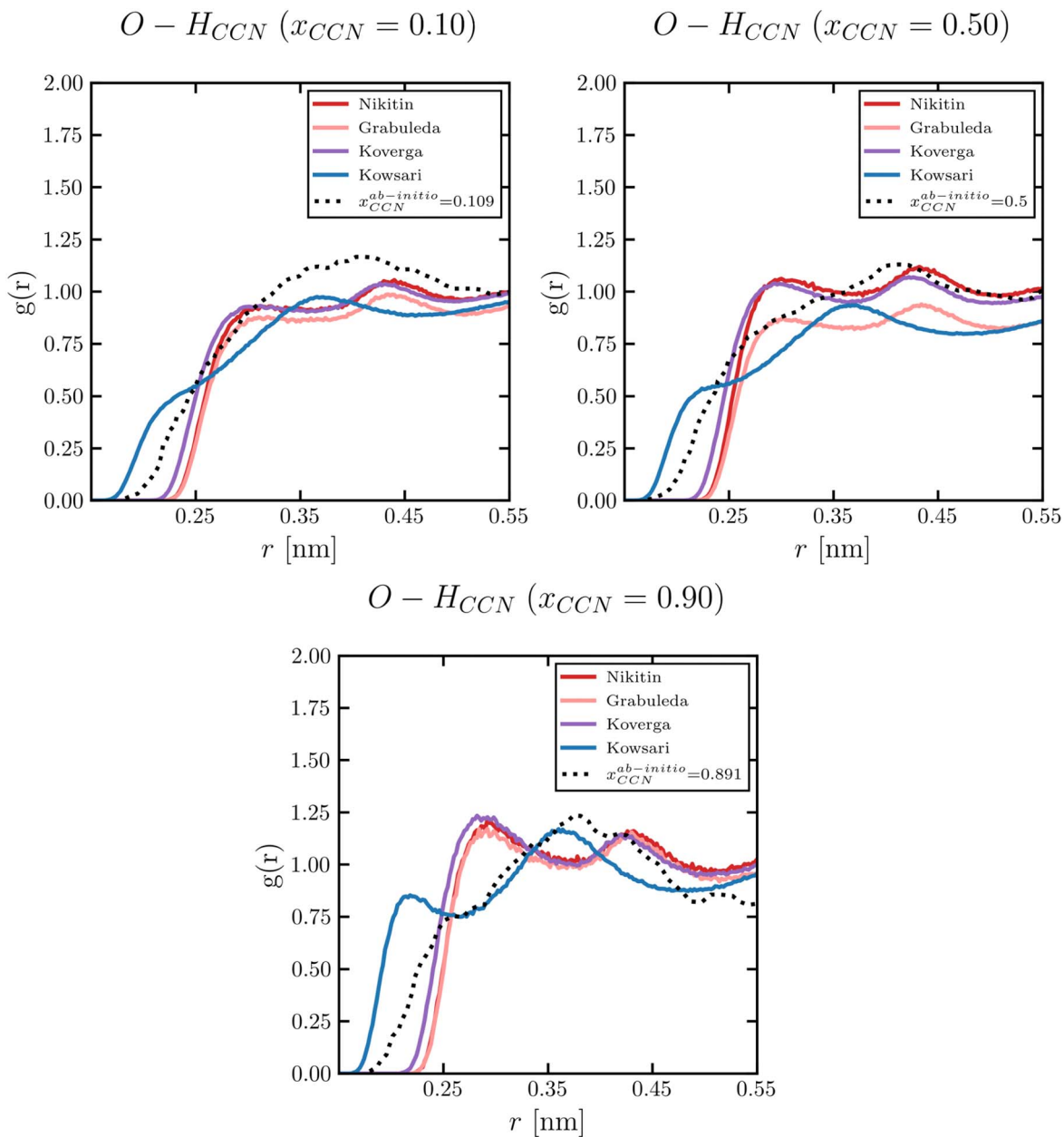


Figure 4. Same as Fig. 2 for oxygen atoms in water and hydrogen atoms in CCN.

In the presence of high macroscopic electric fields, the orientation correlation between neighboring CCN molecules changes qualitatively. This is demonstrated in Fig. 9, which shows contour plots of the CDF between first neighbor molecules (same as Fig. 8) for three different applied fields, $|\mathbf{E}| = 0.1 \text{ V nm}^{-1}\text{nm}$, $0.2 \text{ V nm}^{-1}\text{nm}$, and $0.3 \text{ V nm}^{-1}\text{nm}$. With increasing macroscopic field, the peak corresponding to the antiparallel orientation gradually disappears, and instead, a peak at $\theta = 0^\circ$ (parallel orientation) emerges. The change in orientation explains the slight changes in the radial distribution function $g(r)$ of atom pairs between two CCN molecules as a function of the electric field in Figs. 7b and S9 in SI.

In order to assess whether this is a nonlinear effect, we have computed the integrated angular correlation function, which we define as the radial integral $\int_0^{r_{\text{cut}}} dr g_{CDF}(r, \theta)$, where the upper limit, $r_{\text{cut}} = 0.6 \text{ nm}$ corresponds to the first minimum of the center-of-mass correlation of CCN molecules as discussed above. The result is shown in Fig. 10. The curves clearly show the gradual

transition between a state where neighboring CCN molecules mostly show an antiparallel orientation to a state where they are mostly parallel to each other. They also demonstrate that this is clearly a nonlinear effect: Initially, for small fields, the integrated angular correlation functions are roughly independent of the applied field. Around $E \sim 0.1 \text{ V nm}^{-1}$, they start to change such that the integrated CDF at $\theta = 0^\circ$ (parallel orientation) grows at the expense of the integrated CDF at $\theta = 180^\circ$ (antiparallel orientation).

Hydrogen bond network and micro-heterogeneities.—Finally, we study the structure of the hydrogen bond network in our mixtures, which can give indirect information on potential channels for proton transport in the system. Since classical molecular dynamic simulations do not explicitly account for proton delocalization, the first problem consists in identifying hydrogen bonds or potential hydrogen bonds in classical configurations. Different hydrogen bond definitions have been proposed in the literature.^{64,65} In the present

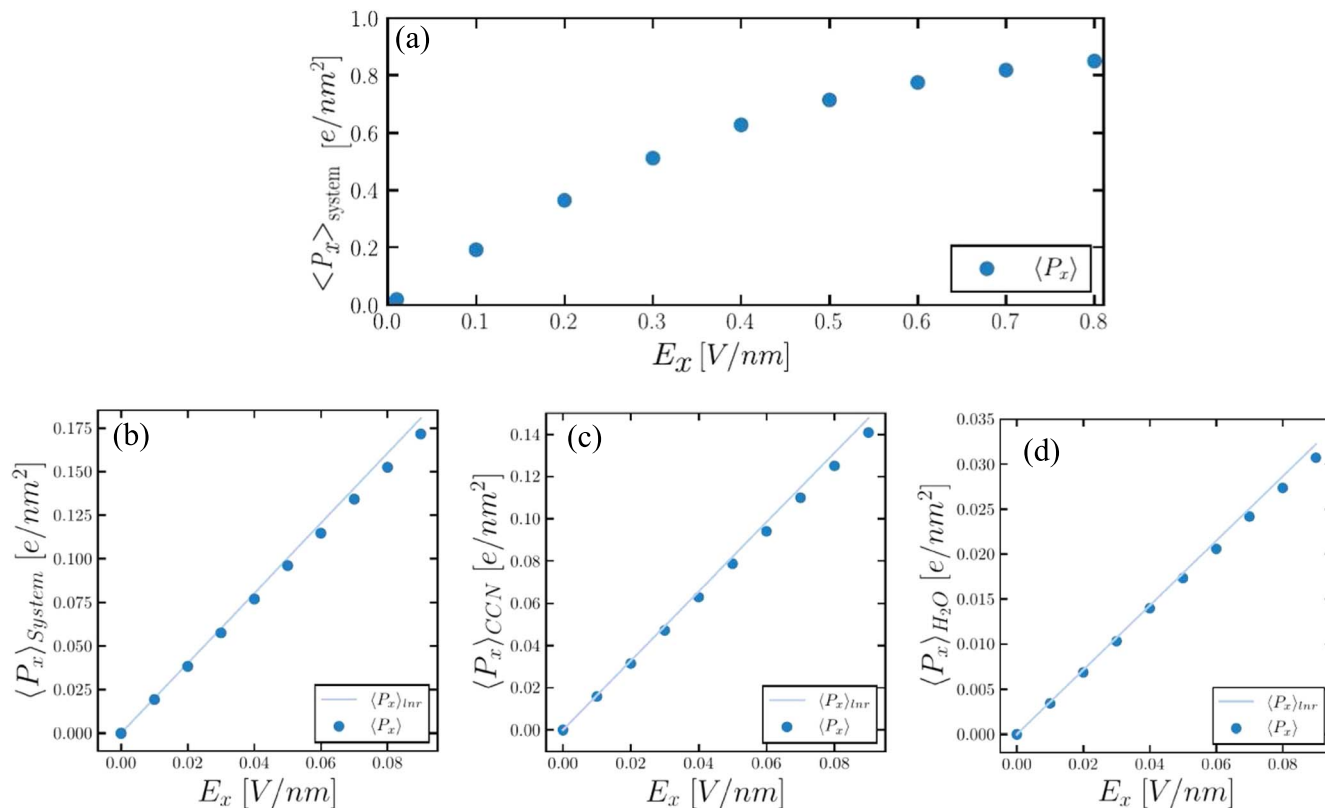


Figure 5. Total polarization (a), (b) and corresponding CCN (c) and water contributions (d) as a function of the macroscopic field. The solid lines show the linear response value obtained from Eq. 4.

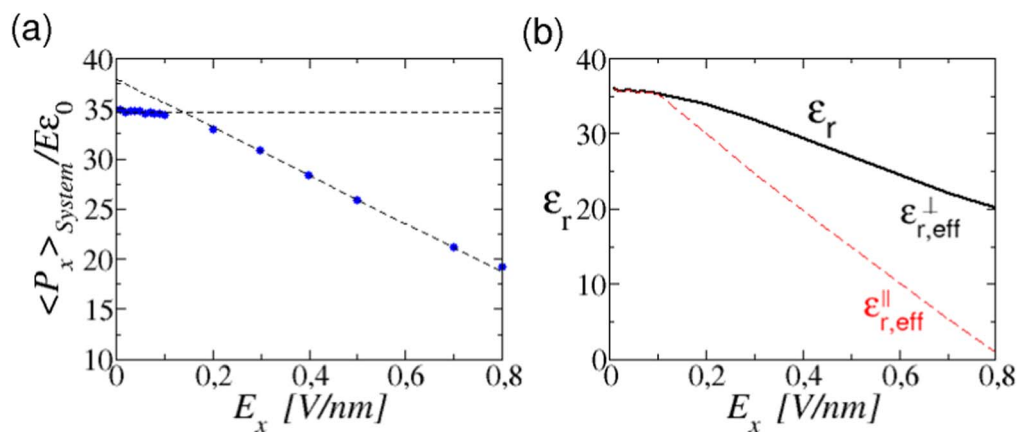


Figure 6. (a) Ratio $\langle P_x \rangle_{\text{system}} / (E \epsilon_0)$ as a function of the macroscopic field. The dashed lines illustrate the crossover from a constant behavior to a linear decay. (b) Resulting dielectric constant and effective dielectric constant.

study, we use the CHIMERA⁶⁶ software to identify the hydrogen bond network. The CHIMERA tool applies a geometric criterion to compute a three dimensional hydrogen bond distribution, and therefore a probability of hydrogen-bond formation, for each hydrogen-bonding site.⁶⁷ Some more details can be found in SI. Once we have identified hydrogen bonds, we can identify clusters and represent hydrogen bond networks via graphs, where the nodes correspond to hydrogen donor and/or acceptor molecules and the edges to hydrogen bonds. We note that in rare cases, the CHIMERA software may assign two hydrogen bonds to the same CCN molecule, see Fig. 11c. Even though such complexes do exist,⁶⁸ the CHIMERA assignment in such cases is most likely wrong. Nevertheless, the analysis provides a useful tool to evaluate the geometric network of the molecules in the system.

Figure 11 shows representative examples of two-dimensional graph descriptions of the hydrogen bond network for CCN-water mixtures at CCN concentrations of (a) $x_{\text{CCN}} = 0.25$ and (b) $x_{\text{CCN}} = 0.75$. Every node represents a molecule, either CCN or water, and every connecting line corresponds to a hydrogen bond. In addition, these clusters might contain cycles of hydrogen-bonded chains. For low CCN concentrations, a single large graph dominates containing many interconnected cycles, whereas tree graphs are abundant at high CCN concentrations. Dangling ends, in this case, mostly correspond to CCN molecules where further hydrogen bonding is impossible. These observations are similar to those reported in Ref. 36 for water/methanol mixtures.

To describe microheterogeneities in these binary mixtures, it is useful to identify sub-classes of hydrogen-bonded clusters inside the

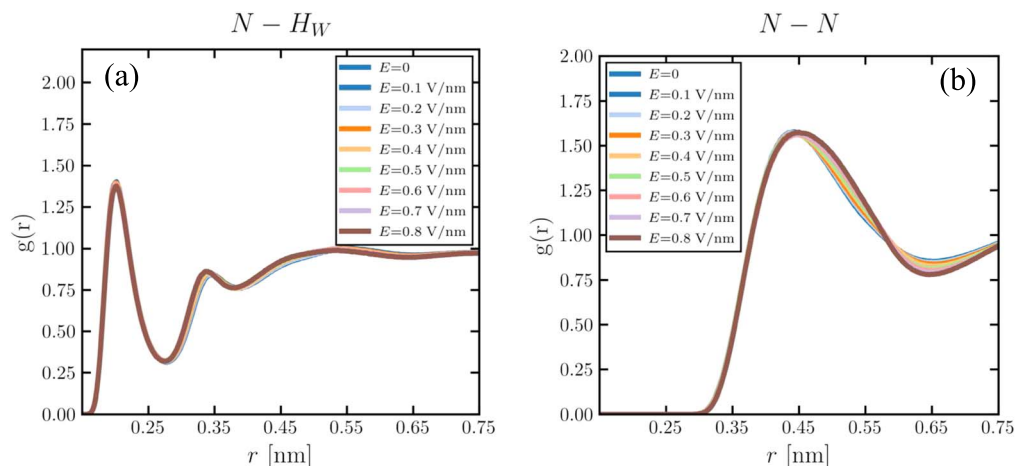


Figure 7. Radial distribution functions at $x_{CCN} = 0.75$ for different electric fields as indicated between (a) nitrogen and water hydrogen, and (b) two nitrogens.

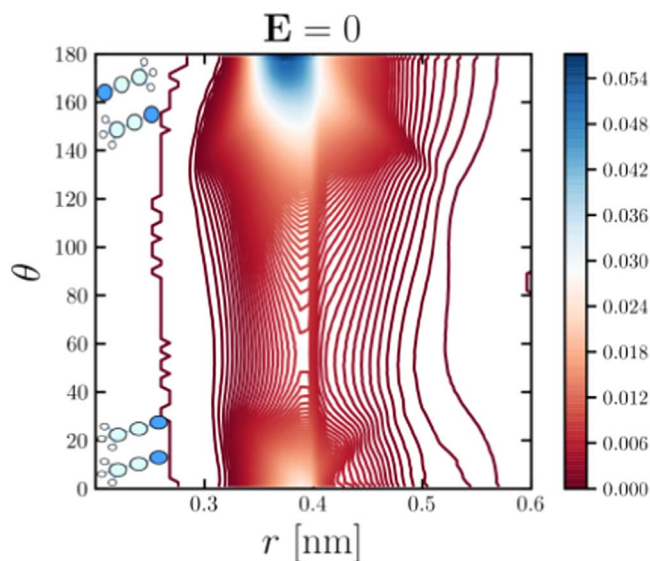


Figure 8. Combined distribution functions (CDFs) between the center of mass of CCN first neighbors and the θ angle between vectors defined along the CCN molecules in CNN-water mixtures at $\mathbf{E} = 0$.

simulation box.⁶⁹ The first sub-class represents the largest cluster, and the other sub-classes represent the smaller ones. Figure 12 shows one example of a large cluster in a configuration taken from a

trajectory of 100 ns at CCN mole fraction $x_{CCN} = 0.75$ in graph representation (a) and in real space (b). One can clearly see that the water molecules in the hydrogen-bonded cluster are mainly inside, and partially surrounded by CCN molecules. Panel (c) in the same figures specifically highlights molecules that belong to cycles in hydrogen-bond network. We note that in rare cases, the Chimera may wrongly assign two hydrogen bonds to the same CCN molecule. This can be seen in one of the cycles (light red) which contains, shown as largest bead, a CCN molecule.

To quantify the properties of the hydrogen bond network and the impact of macroscopic electric field, we have calculated histograms of the number of molecules $N_{molecules}$ in the largest hydrogen bond cluster of the configurations at $x_{CCN} = 0.75$. The results are shown in Fig. 13. The curves exhibit a pronounced maximum around $N_{molecules} \sim 60$, followed by a long tail that decays to zero at $N_{molecules} \sim 200 - 250$. The total number of water molecules in these configurations is around 2000, hence even the largest cluster contains only a small fraction. Apart from a very small shift to larger $N_{molecules}$, the shape of the curves is almost unaffected by macroscopic fields.

Furthermore, we have also analyzed the cycles (see Fig. 12c) in the largest clusters of our configurations and evaluated histograms of the number of molecules that constitute a cycle. The results are shown in Fig. 14. Our results for electric field zero ($\mathbf{E} = 0$) are consistent with an earlier study of Bergman and Laaksonen,¹⁵ who determined histograms for the lengths of all cycles in the hydrogen bond network of water/CCN mixtures. The shape of the histograms is very similar, and Bergman and Laaksonen also report a maximum at cycle length five. Here, we find that applying a macroscopic field

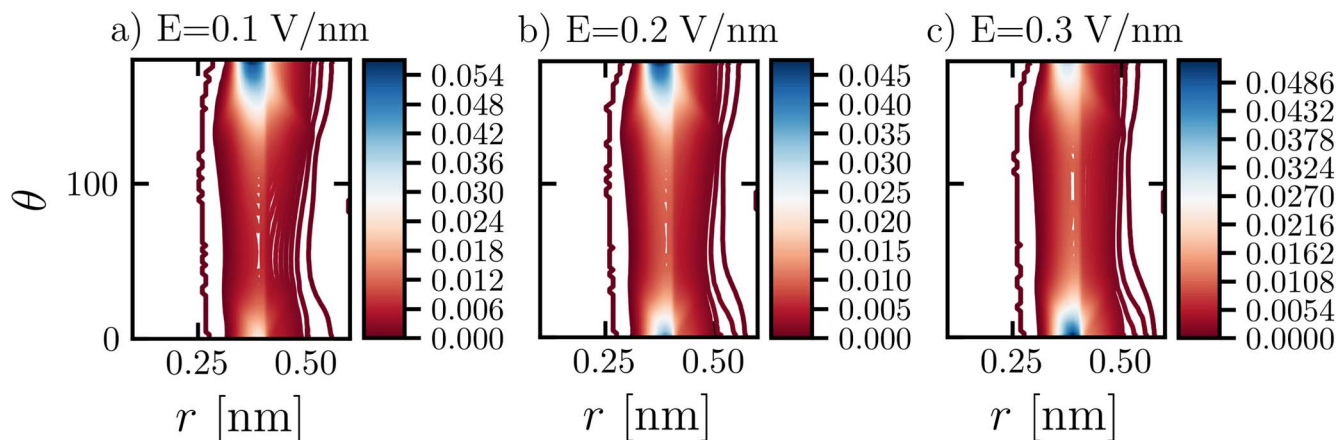


Figure 9. Same as Fig. 8 for different macroscopic fields E as indicated.

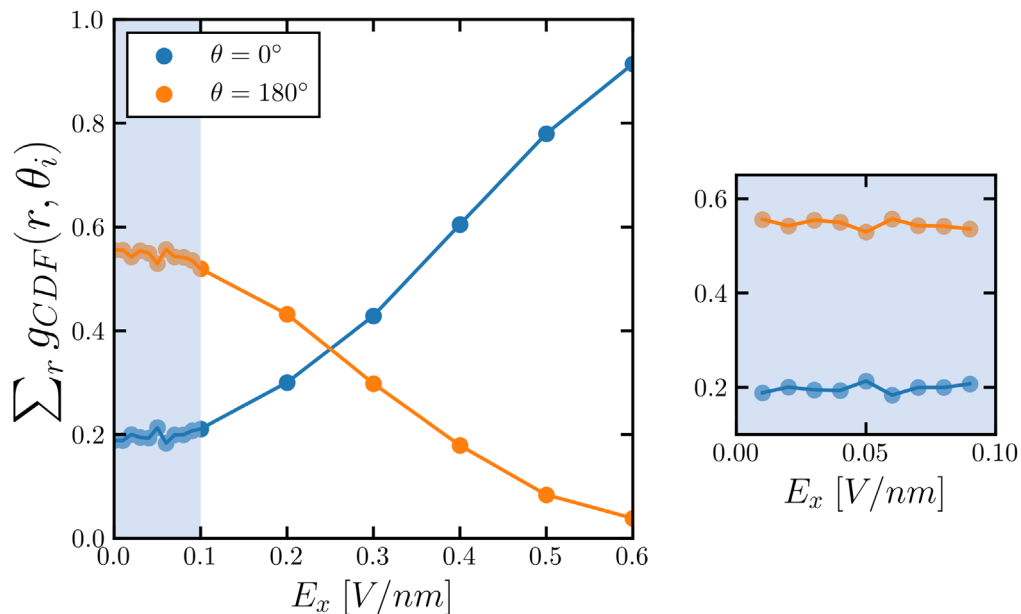


Figure 10. Radially integrated combined distribution function from Fig. 9 at the two angles $\theta = 0^\circ$ and $\theta = 180^\circ$ as a function of macroscopic field E_x . The right panel shows a blowup at small macroscopic fields E_x .

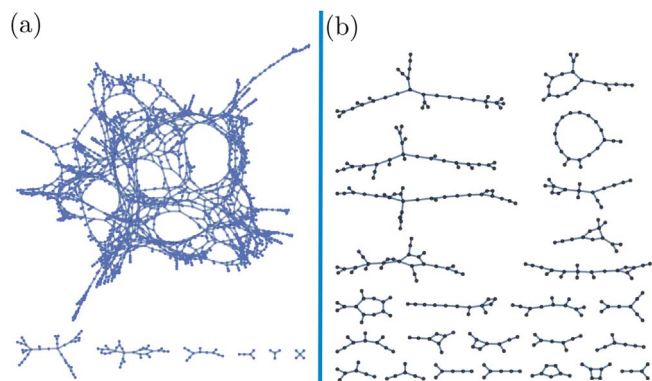


Figure 11. Examples of planar representations of hydrogen bond networks via graphs. Each node corresponds to a molecule of water or acetonitrile. For every mole fraction, the hydrogen bond network forms clusters. Panel (a) shows an example for a configuration at $x_{CCN} = 0.25$ containing one large and highly interconnected cluster and several rather small clusters. Panel (b) shows an example for a configuration at $x_{CCN} = 0.75$ showing many smaller elongated and often tree-like clusters.

has no impact at all on the distribution and number of cycles in the largest cluster.

Summary and Conclusions

In the present work, we have studied the impact of macroscopic electric fields on the structure of water/acetonitrile mixtures. We find that these systems exhibit a nearly linear response to electric fields up to field amplitudes of around $E \sim 0.1$ V/nm. The most prominent signature of nonlinear behavior is a reorientation of neighboring CCN molecules from antiparallel, which is predominant at field zero, to parallel, which dominates at very high fields. However, the characteristics of the hydrogen bond network seem largely unaffected by this up to electric field strengths which are high above the dielectric breakdown limit in real systems.

In this context, we have also investigated the signatures of microheterogeneities in the hydrogen bond network of the water/acetonitrile mixtures at high acetonitrile content. We found that the connected hydrogen bond clusters in the mixtures correspond to

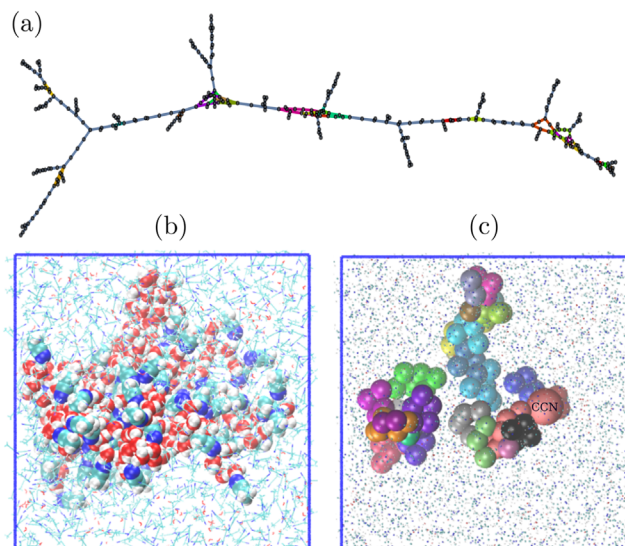


Figure 12. Example of a large hydrogen-bonded cluster in a CCN-water mixture at $x_{CCN} = 0.75$, as determined by the Chimera tool.⁶⁶ (a) Graph representation. Dangling ends correspond to CCN molecules. Different cycles in the graph are marked by different colors. (b) Real space all-atom representation of the molecules belonging to this network. Oxygen atoms in water are red, and nitrogen atoms in CCN are blue. (c) Real space coarse-grained representation of cycles inside the same graph. Every bead corresponds to a molecule. Different colors correspond to different cycles, the color coding is the same as in (a). The largest bead represents a CCN molecule, which is part of a cycle because two hydrogen bonds were assigned to it (most likely wrongly, see text).

compact clusters in real space which are partially surrounded by acetonitrile molecules, which correspond to dangling ends in the graph representation of the cluster. This supports the view that acetonitrile acts as a confinement matrix for water clusters.

The present study was partly motivated by a recent intriguing observation in narrow-gap electrolysis cells,⁷⁰ where it was found that such mixed solvents may support currents even in the absence of supporting electrolyte if the gaps are very small, i.e. the applied fields are high. In these experimental settings, the gap width is of the

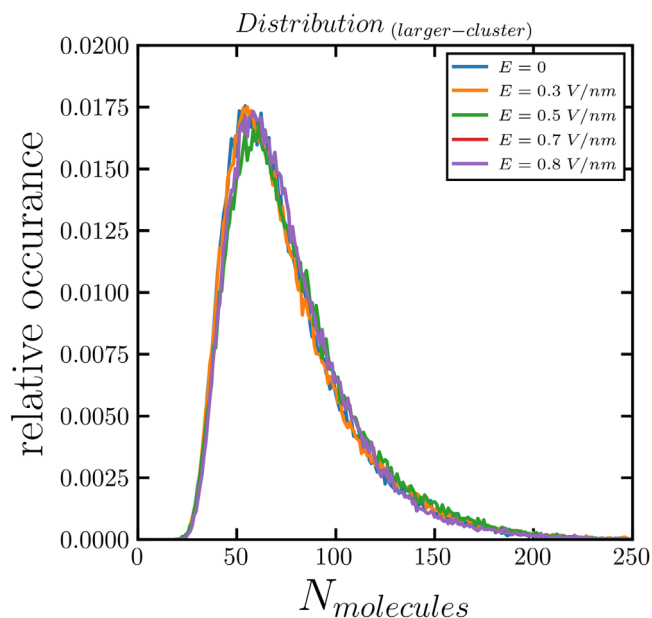


Figure 13. Distribution of the number of molecules $N_{molecules}$ in the largest hydrogen bond cluster of configurations at $x_{CCN} = 0.75$ for different applied electric fields as indicated.

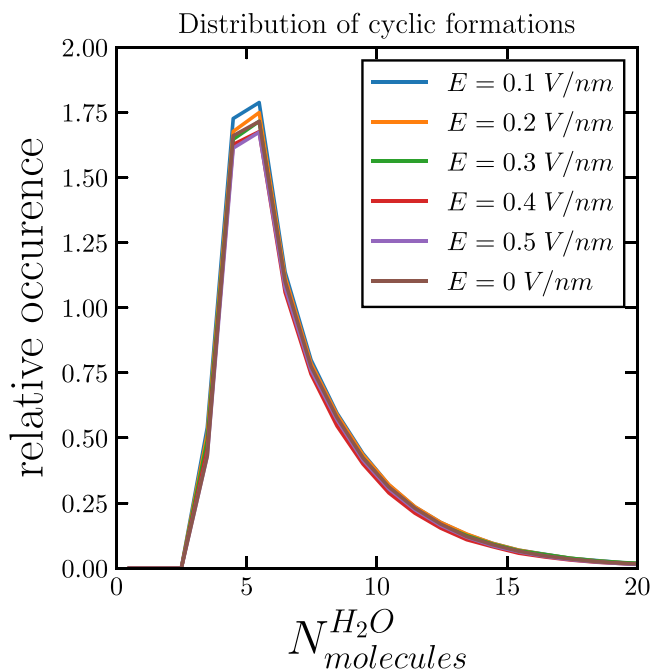


Figure 14. Histogram of the number of molecules belonging to a cycle formation within the largest cluster of a configuration for different macroscopic electric fields as indicated. Cycles with 5 molecules dominate.


order of millimeters and the fields thus never exceed $1 \text{ V}/\mu\text{m}$, which is deep in the linear response regime according to the present study. Our study does not provide any evidence of significant structural changes in this regime. Therefore, we must conclude that we cannot explain the experimental results. Further studies will be necessary which possibly will have to include the effect of electrodes and impurities.

Acknowledgments

This work was funded by the Deutsche Forschungsgemeinschaft (DFG, German research foundation) within research unit FOR 2982

(UNODE), project number 413163866. A.S. is an associate member of the RTG 2516, project number 405552959. N.C.F.M. acknowledge the ECHELON project from the Carl Zeiss Foundation for financial support. We thank Siegfried Waldvogel and Maximilian Hielscher for inspiring this work and Giovanni Settanni for helpful discussions.

ORCID

Anastasios I. Sourpis  <https://orcid.org/0000-0003-1192-798X>
Nancy C. Forero-Martinez  <https://orcid.org/0000-0001-8903-7878>
Friederike Schmid  <https://orcid.org/0000-0002-5536-6718>

References

1. Y. Marcus, "The structure of and interactions in binary acetonitrile plus water mixtures." *J. Phys. Org. Chem.*, **25**, 1072 (2012).
2. C. Moreau and G. Douhéret, "Thermodynamic behavior of water-acetonitrile mixtures excess volumes and viscosities." *Thermochim. Acta*, **13**, 385 (1975).
3. M. Stähelin, C. R. Moylan, D. M. Burland, A. Willetts, J. E. Rice, D. P. Shelton, and E. A. Donley, "A comparison of calculated and experimental hyperpolarizabilities for acetonitrile in gas and liquid phases." *J. Chem. Phys.*, **98**, 5595 (1993).
4. J. E. Bertie and Z. Lan, "Liquid water-acetonitrile mixtures at 25 °C: the hydrogen-bonded structure studied through infrared absolute integrated absorption intensities." *J. Phys. Chem. B*, **101**, 4111 (1997).
5. D. Venables and C. Schmittenmaer, "Spectroscopy and dynamics of mixtures of water with acetone, acetonitrile, and methanol." *J. Chem. Phys.*, **113**, 11222 (2000).
6. I. Bako, T. Megyes, and G. Palinkas, "Structural investigation of water-acetonitrile mixtures: An ab initio, molecular dynamics and X-ray diffraction study." *Chem. Phys.*, **316**, 235 (2005).
7. I. Bako, T. Megyes, T. Grosz, G. Palinkas, and J. Dore, "Structural investigation of water-acetonitrile mixtures: Small-angle and wide-angle neutron diffraction study compared to molecular dynamics simulation." *J. Mol. Liq.*, **125**, 174 (2006).
8. F. Ding, Z. Hu, Q. Zhong, K. Manfred, R. R. Gattass, M. R. Brindza, J. T. Fourkas, R. A. Walker, and J. D. Weeks, "Interfacial organization of acetonitrile: simulation and experiment." *J. Phys. Chem. C*, **114**, 17651 (2010).
9. M. Nagasaka, H. Yuzawa, and N. Kosugi, "Microheterogeneity in aqueous acetonitrile solution probed by soft x-ray absorption spectroscopy." *J. Phys. Chem. B*, **124**, 1259 (2020).
10. S. R. Cohen, M. Plazanet, S. Rols, D. J. Voneshen, J. T. Fourkas, and B. Coasne, "Structure and dynamics of acetonitrile: molecular simulation and neutron scattering." *J. Mol. Liq.*, **348**, 118423 (2022).
11. M. Matsumoto, H. Tanaka, and K. Nakanishi, "Acetonitrile pair formation in aqueous solution." *J. Chem. Phys.*, **99**, 6935 (1993).
12. Y. Satoh and K. Nakanishi, "Theoretical studies of acetonitrile-water mixtures / Monte Carlo simulation." *Fluid Phase Equilibria*, **104**, 41 (1995).
13. H. Reis, M. G. Papadopoulos, and A. Avramopoulos, "Calculation of the microscopic and macroscopic linear and nonlinear optical properties of liquid acetonitrile. i. accurate molecular properties in the gas phase and susceptibilities of the liquid in onager's reaction-field model." *J. Phys. Chem. C*, **107**, 3907 (2003).
14. H. Kovacs and A. Laaksonen, "Molecular-dynamics simulation and NMR-study of water acetonitrile mixtures." *J. Am. Chem. Soc.*, **113**, 5596 (1991).
15. D. Bergman and A. Laaksonen, "Topological and spatial structure in the liquid-water-acetonitrile mixture." *Phys. Rev. E*, **58**, 4706 (1998).
16. R. Mountain, "Molecular dynamics study of water-acetonitrile mixtures." *J. Phys. Chem. A*, **103**, 10744 (1999).
17. C. Oldiges, K. Wittler, T. Tonsing, and A. Alijah, "MD calculated structural properties of clusters in liquid acetonitrile/water mixtures with various contents of acetonitrile." *J. Phys. Chem. A*, **106**, 7147 (2002).
18. A. Avramopoulos, M. G. Papadopoulos, and H. Reis, "Calculation of the microscopic and macroscopic linear and nonlinear optical properties of liquid acetonitrile. ii. local fields and linear and nonlinear susceptibilities in quadrupolar approximation." *J. Phys. Chem. B*, **111**, 2546 (2007).
19. A. Y. Zasetsky, S. V. Petelina, A. K. Lyashchenko, and A. S. Lileev, "Computer simulation study of rotational diffusion in polar liquids of different types." *J. Chem. Phys.*, **133**, 134502 (2010).
20. R. D. Mountain, "Microstructure and hydrogen bonding in water-acetonitrile mixtures." *J. Phys. Chem. B*, **114**, 16460 (2010).
21. J. Chen and P. H. L. Sit, "Ab initio study of the structural properties of acetonitrile-water mixtures." *Chem. Phys.*, **457**, 87 (2015).
22. M. J. Makowski, A. C. Stern, J. C. Hemminger, and D. J. Tobias, "Orientation and structure of acetonitrile in water at the liquid-vapor interface: a molecular dynamics simulation study." *J. Phys. Chem. C*, **120**, 17555 (2016).
23. S. Pothoczki and L. Pusztai, "Intermolecular orientations in liquid acetonitrile: new insights based on diffraction measurements and all-atom simulations." *J. Mol. Liq.*, **225**, 160 (2017).
24. I. N. Daniels, Z. Wang, and B. B. Laird, "Dielectric properties of organic solvents in an electric field." *J. Phys. Chem. C*, **121**, 1025 (2017).
25. S. M. Aguilera-Segura, F. Di Renzo, and T. Mineva, "Structures, intermolecular interactions, and chemical hardness of binary water-organic solvents: a molecular dynamics study." *J. Mol. Model.*, **24**, 292 (2018).
26. Z. S. Vokacova and E. Pluharova, "Understanding structure and dynamics of organic liquid mixtures by molecular simulations." *J. Mol. Liq.*, **288**, 110778 (2019).

27. O. R. Gittus, P. Albella, and F. Bresme, "Polarization of acetonitrile under thermal fields via non-equilibrium molecular dynamics simulations." *J. Chem. Phys.*, **153**, 204503 (2020).
28. H. J. Böhm, I. R. McDonald, and P. A. Madden, "An effective pair potential for liquid acetonitrile." *Mol. Phys.*, **49**, 347 (1983).
29. W. L. Jorgensen and J. M. Briggs, "Monte-Carlo simulations of liquid acetonitrile with a 3-site model." *Mol. Phys.*, **63**, 547 (1988).
30. X. Grabuleda, C. Jaime, and P. Kollman, "Molecular dynamics simulation studies of liquid acetonitrile: new six-site model." *J. Comput. Chem.*, **21**, 901 (2000).
31. A. M. Nikitin and A. P. Lyubartsev, "New six-site acetonitrile model for simulations of liquid acetonitrile and its aqueous mixtures." *J. Comput. Chem.*, **28**, 2020 (2007).
32. V. A. Kovrega, O. M. Korsun, O. N. Kalugin, B. A. Marekha, and A. Idrissi, "A new potential model for acetonitrile: insight into the local structure organization." *J. Mol. Liq.*, **233**, 251 (2017).
33. M. H. Kowsari and L. Tohidifar, "Systematic Evaluation and Refinement of Existing All-Atom Force Fields for the Simulation of Liquid Acetonitrile." *J. Comput. Chem.*, **39**, 1843 (2018).
34. R. Berthoin, A. Serva, K. G. Reeves, E. Heid, C. Schröder, and M. Salanne, "Solvation of anthraquinone and TEMPO redox-active species in acetonitrile using a polarizable force field." *J. Chem. Phys.*, **155**, 074504 (2021).
35. J. G. McDaniel, "Polarization effects in binary [BMIM+][BF4-]/1,2-dichloroethane, acetone, acetonitrile, and water electrolytes." *J. Phys. Chem. B*, **122**, 4345 (2018).
36. I. Bakó, T. Megyes, S. Bálint, T. Grósz, and V. Chihai, "Water-methanol mixtures: topology of hydrogen bonded network." *Phys. Chem. Chem. Phys.*, **10**, 5004 (2008).
37. G. Cassone, P. V. Giaquinta, F. Saija, and A. M. Saitta, "Liquid methanol under a static electric field." *J. Chem. Phys.*, **142**, 054502 (2015).
38. G. Cassone, "Nuclear quantum effects largely influence molecular dissociation and proton transfer in liquid water under an electric field." *J. Phys. Chem. Lett.*, **11**, 8983 (2020).
39. G. Cassone, A. Sofia, J. Sponer, A. M. Saitta, F. Saija, and Ab Initio, "Molecular dynamics study of methanol-water mixtures under external electric fields." *Molecules*, **25**, 3371 (2020).
40. G. Cassone, J. Sponer, F. Saija, and Ab Initio, "Molecular dynamics studies of the electric-field-induced catalytic effects on liquids." *Top. Catal.*, **65**, 40 (2022).
41. V. Conti Nibali, S. Maiti, F. Saija, M. Heyden, and G. Cassone, "Electric-field induced entropic effects in liquid water." *J. Chem. Phys.*, **158**, 184501 (2023).
42. C. A. Petroff, G. Cassone, J. Šponer, and G. R. Hutchison, "Intrinsically polar piezoelectric self-assembled oligopeptide monolayers." *Adv. Mater.*, **33**, 2007486 (2021).
43. S. Shaik, D. Mandal, and R. Ramanan, "Oriented electric fields as future smart reagents in chemistry." *Nat. Chem.*, **8**, 1091 (2016).
44. S. Shaik, D. Danovich, J. Joy, Z. Wang, and T. Stuyver, "Electric-field mediated chemistry: uncovering and exploiting the potential of (oriented) electric fields to exert chemical catalysis and reaction control." *J. Am. Chem. Soc.*, **142**, 12551 (2020).
45. G. Cassone, A. Sofia, G. Rinaldi, and J. Sponer, "Catalyst-free hydrogen synthesis from liquid ethanol: an ab initio molecular dynamics study." *J. Phys. Chem. C*, **123**, 9202 (2019).
46. B. Hess, C. Kutzner, D. van der Spoel, and E. Lindahl, "GROMACS 4: algorithms for Highly Efficient, Load-Balanced, and Scalable Molecular Simulation." *J. Chem. Theory Comput.*, **4**, 435 (2008).
47. H. J. C. Berendsen, J. P. M. Postma, W. F. van Gunsteren, and J. Hermans, *Interaction Models for Water in Relation to Protein Hydration*, ed. B. Pullman (Springer Netherlands, Dordrecht), p. 331 (1981).
48. W. L. Jorgensen, J. Chandrasekhar, J. D. Madura, R. W. Impey, and M. L. Klein, "Comparison of simple potential functions for simulating liquid water." *J. Chem. Phys.*, **79**, 926 (1983).
49. M. Stengel, N. A. Spaldin, and D. Vanderbilt, "Electric displacement as the fundamental variable in electronic-structure calculations." *Nat. Phys.*, **5**, 304 (2009).
50. C. Zhang and M. Sprik, "Computing the dielectric constant of liquid water at constant dielectric displacement." *Phys. Rev. B*, **93**, 144201 (2016).
51. C. Zhang, J. Hutter, and M. Sprik, "Computing the kirkwood g-factor by combining constant maxwell electric field and electric displacement simulations: application to the dielectric constant of liquid water." *J. Phys. Chem. Lett.*, **7**, 2696 (2016).
52. B. Hess, H. Bekker, H. J. C. Berendsen, and J. G. E. M. Fraaije, "LINCS: a linear constraint solver for molecular simulations." *J. Comput. Chem.*, **18**, 1463 (1997).
53. G. Bussi, D. Donadio, and M. Parrinello, "Canonical sampling through velocity rescaling." *J. Chem. Phys.*, **126**, 014101 (2007).
54. T. Darden, D. York, and L. Pedersen, "Particle mesh Ewald: An $N \log(N)$ method for Ewald sums in large systems." *J. Chem. Phys.*, **98**, 10089 (1993).
55. M. Ormö, A. B. Cubitt, K. Kallio, L. A. Gross, R. Y. Tsien, and S. J. Remington, "Crystal structure of the aequorea victoria green fluorescent Protein." *Science*, **273**, 1392 (1996).
56. L. Martínez, R. Andrade, E. G. Birgin, and J. M. Martínez, "PACKMOL: a package for building initial configurations for molecular dynamics simulations." *J. Comput. Chem.*, **30**, 2157 (2009).
57. M. Brehm, M. Thomas, S. Gehrke, and B. Kirchner, "TRAVIS free analyzer for trajectories from molecular simulation." *J. Chem. Phys.*, **152**, 164105 (2020).
58. W. D. Cornell, P. Cieplak, C. I. Bayly, I. R. Gould, K. M. Merz, D. M. Ferguson, D. C. Spellmeyer, T. Fox, J. W. Caldwell, and P. A. Kollman, *A Second Generation Force Field for the Simulation of Proteins, Nucleic Acids, and Organic Molecules* (ACS Publications) (2002).
59. J. D. Jackson, *Classical Electrodynamics* (Wiley, New York) 3rd ed. (1998).
60. S. W. de Leeuw, J. W. Perram, E. R. Smith, and J. S. Rowlinson, "Simulation of electrostatic systems in periodic boundary conditions. I. Lattice sums and dielectric constants." *Proc. R. Soc. London*, **373**, 27 (1980).
61. J. Caillol, "Comments on the numerical simulations of electrolytes in periodic boundary conditions." *J. Chem. Phys.*, **101**, 6080 (1994).
62. L. G. Gagliardi, C. B. Castells, C. Rafols, M. Roses, and E. Bosch, "Static dielectric constants of acetonitrile/water mixtures at different temperatures and debye Hückel A and a_0B parameters for activity coefficients." *J. Chem. Eng. Data*, **52**, 1103 (2007).
63. K. Schönbach, J. Kolb, S. Xiao, S. Katsuki, Y. Minamitani, and R. Joshi, "Electrical breakdown of water in microgaps." *Plasma Sources Sci. Technol.*, **17**, 024010 (2008).
64. M. Matsumoto, "Relevance of hydrogen bond definitions in liquid water." *J. Chem. Phys.*, **126**, 054503 (2007).
65. I. Bakó, D. Csókás, and S. Pothoczki, "Molecular aggregation in liquid water: Laplace spectra and spectral clustering of H-bonded network." *J. Mol. Liq.*, **327**, 114802 (2021).
66. E. F. Pettersen, T. D. Goddard, C. C. Huang, G. S. Couch, D. M. Greenblatt, E. C. Meng, and T. E. Ferrin, "UCSF Chimera—a visualization system for exploratory research and analysis." *J. Comput. Chem.*, **25**, 1605 (2004).
67. J. E. J. Mills and P. M. Dean, "Three-dimensional hydrogen-bond geometry and probability information from a crystal survey." *J. Comput. Aided Mol. Des.*, **10**, 607 (1996).
68. R. Gopi, N. Ramanathan, and K. Sundararajan, "Acetonitrile-water hydrogen-bonded interaction: matrix-isolation infrared and ab initio computation." *J. Mol. Struct.*, **1094**, 118 (2015).
69. N. Dubouis, A. Serva, R. Berthoin, G. Jeanmairat, B. Porcheron, E. Salager, M. Salanne, and A. Grimaud, "Tuning water reduction through controlled nanoconfinement within an organic liquid matrix." *Nat. Catal.*, **3**, 656 (2020).
70. C. Gütz, A. Stenglein, and S. R. Waldvogel, "Highly Modular Flow Cell for Electroorganic Synthesis." *Org. Process Res. Dev.*, **21**, 771 (2017).